Indian Journal of Chemical Technology
Vol. 30, September 2023, pp. 643-655
DOI: 10.56042/ijct.v30i5.5193

Adsorptive removal of malachite green using ferromagnetic sterculia gum – graft-poly(n-isopropylacrylamide-co-acrylamide)/magnetite nanocomposite

S K Tank[1,2] & N Sharma[1]*

[1]Department of Physical Sciences, Sant Baba Bhag Singh University, Jalandhar, Punjab 144 030, India
[2]Department of Chemistry, Kanya Maha Vidyalaya, Jalandhar, Punjab 144 001, India
*E-mail: nishi.hpu@gmail.com

Received 7 August 2022; accepted 3 April 2023

In present scenario, anthropogenic activities have degraded the quality of water bodies to an unbearable level. Discharge of untreated industrial and other effluents have made the water unconsumable. Present work is an attempt to fabricate new stimuli responsive adsorbent based on natural exudate gum sterculia, an indigenous natural gum for uptake of a cationic dye malachite green. Magnetic field responsive terculia gum–graft-poly(n-isopropylacrylamide-co-acrylamide) nanocomposite have been prepared and assessed it as adsorbents for enrichment of malachite green from aqueous solution. The nanocomposite is characterized by FTIR, TG-DTA, VSM and swelling studies. The VSM results have shown is superparamagnetic behaviour of nanocomposite with saturation magnetization of 1.5065 emu/g. The adsorption follows Temkin isotherm and results indicate maximum adsorption capacity of 19.977 (98.78%) malachite green. The desorption studies demonstrates excellent recovery ability of nanocomposite. The adsorption study confirms the prospective applications of polysaccharide based magnetic hydrogel for the fruitful and greener disposal of cationic dyes.

Keywords: Adsorption, Ferromagnetic, Magnetite, Malachite green, Recycling, Sterculia gum

Technological advancement has led to the growth of various industries like paper, cosmetics, printing, textile, plastic, pharmaceutical and food that make generous use of dyes. Effluents released from these industries are loaded with dyes that are highly soluble in water and toxic with lower degradation ability[1,2]. Additionally these dyes being synthetic, carcinogenic and mutagenic in nature have alarming threats to the human health as well as to the aquatic biota thereby disturbing the ecological balance[3,4]. Hence, the treatment of these precarious dyes is vital area of research.

Malachite green consists of a macrocyclic ring, an N-methylated diaminotriphenylmethane and employed for dying fabrics, paper and leather. It is also used as a biological stain and as an anti-fungal agent in aquaculture[5]. However the dye affect human immune system and has carcinogenic, mutagenic, teratogenic behaviour, chromosomal fracture ability, and respiratory toxicity[6,7].

From time to time different conventional methods namely ion exchange, biodegradation, coagulation-flocculation, adsorption, oxidation, photocatalysis and separation using membrane are reported for the degradation of dyes[8,9]. Amongst these methods, adsorption is extensively employed techniques on account of its high potency, inexpensiveness, facile handling, regeneration ability and environment friendly nature[10]. Classical adsorbents such as silica gel, activated charcoal, zeolites etc. show outstanding adsorption capacity for the enrichment of organic dyes. But high prices, lower efficiency and difficult recycling make it impossible to cater the increasing demand of water purification processes. Hence, to develop effective and viable adsorbents for controlling and removing various organic dyes from polluted water is the need of the hour. Polymeric hydrogels especially chemically functionalized hydrogels have revolutionized the dye enrichment strategies. Due to uncontrolled water pollution, and the rising demand to acquire better selectivity, stimuli responsiveness and efficient reusability, more efficient adsorbents are desirable.

In recent years, contemporary research trend focuses on the development of nanosized adsorbent having large surface area that plays pioneering role in facile adsorption. Magnetic nanocomposites using polymer such as alginate, dextrin, gum Arabic, gum xanthan, etc. has been synthesized and successfully employed for enrichment of dye and toxic metal ions from the aqueous solutions[11-13]. Iron oxide magnetic

nanoparticles offers additional benefit of easy separation from the solution by external magnetic field[14,15] and provides more sites for dye bonding[16]. Recently several researchers have reported the use of magnetic iron oxide (Fe_3O_4) nanoparticles as good adsorbents owing to their excellent, paramagnetic behaviour, low toxicity, increased surface-to-volume ratio and simple separation using a magnet[17].

Keeping in view such advantages of iron based nanoparticles, various studies have been centralized to develop magnetic responsive hydrogel for dye enrichment. Biomagnetic membrane capsules using a polyvinyl alcohol and sodium alginate were prepared for adsorbing cationic malachite green dye from water[18]. Xanthan gum / Fe_3O_4 magnetic nanocomposite was reported for effective removal of malachite green (MG)[19]. Removal of MG was also achieved using polyacrylamide-*g*-chitosan γ-Fe_2O_3 nanocomposite[20]. Hydrogel grated using starch, acrylamide, graphene oxide and hydroxyapatite were used for malachite green removal[21]. Another hydrogel based on β-cyclodextrin and magnetic graphene oxide was applied for the removal of methylene blue, safranine T, rhodamine B and malachite green from aqueous solution[22]. Taking into account the toxic consequences of MG, and excellent adsorption capacity of Fe_3O_4 nanocomposites, present study deals with the fabrication of highly efficient sterculia gum based magnetic hydrogel nanocomposite for the removal of malachite green from the aqueous solution.

Sterculia gum is a high molecular weight polysaccharide gum with complex chemical framework consisting of L-rhamnose and D-galactose along with complex carbohydrates D-glucuronic acid and D-galacturonic acid[23]. In this context, the pivotal goal of the present work is to synthesize sterculia gum – graft- poly(n-isopropylacrylamide-co-acrylamide) Fe_3O_4 magnetic nanocomposite with monomers PNIPAM and AAm via free radical graft copolymerization method and by *in situ* integration of magnetite nanoparticles inside the polymer network. The nanocomposite was evaluated for the adsorptive enrichment of cationic dye malachite green in context of adsorption isotherm, kinetic, and thermodynamic studies. Finally desorption experiments were also conducted to investigate regeneration and reusability of adsorbents.

Experimental Section

Material

Sterculia gum was obtained from Sigma Aldrich (USA), N-isopropylacrylamide (NIPAM) from Alfa Aesar (China), acrylamide (AAM), tetramethylethylenediamine (TEMEDA), N,N, methylenebisacrylamide (N,N-MBA) from Molychem (India), Ammonium persulfate (APS) and (MG) from Renkam (India), potassium chloride, potassium dihydrogen phosphate and sodium hydroxide was procured from S.D Fine Chemicals (India), hydrochloric acid, iron(II) chloride tetrahydrate and iron(III) chloride hexahydrate from Merck (India), ammonium hydroxide (25%) from Qualigens (India). Buffer solutions (pH 4, 7, 9.2) were prepared as per Indian pharmacopeia 1996 guidelines.

Synthesis of sterculia gum–graft-poly(n-isopropylacrylamide-co-acrylamide) hydrogel

0.4 g of sterculia gum was dissolved in 10 mL distilled water and allowed to stir at room temperature to obtain a homogeneous solution. Then AAM (2.81 mmol) and NIPAM (1.76 mmol) were added and stirred for 10 min. Then crosslinker MBA (0.12 mmol), APS (0.087 mmol) and TEMEDA (0.22 mmol) were added and further stirred for 20 min. The polymerization reaction was continued for 2 h at 35°C in a constant water bath until SG-*g*-P(NIPAM-*co*-AAM) hydrogel was obtained. The resulting hydrogel was immersed in distilled water for 16 h to remove the unreacted components followed by purification with methyl alcohol and drying in oven at 40°C. It was coded as SG-*g*-P(NIPAM-*co*-AAM).

Synthesis of sterculia gum–graft-poly(n-isopropylacrylamide-co-acrylamide)/magnetite nanocomposite

The magnetic nanocomposite was synthesized according to the procedure reported in literature[24]. Typically about 0.5 g of dried SG-*g*-P(NIPAM-*co*-AAM) gel was soaked in a hard glass test tube having 100 mL solution of $FeCl_3.6H_2O$ (2.1 g) and $FeCl_2.4H_2O$ (5.8 g) then equilibrated for 24 h. Then the resulting swollen gel loaded with Fe^{2+} and Fe^{3+} was then transferred in 100 mL 0.5 M ammonium hydroxide and kept in it for 18 h. The colour of hydrogel varied from brown to intense black implying incorporation of magnetic nanoparticles in the polymer composite. The black coloured gel was cleaned thoroughly with double distilled water in order to get rid off any unreacted constituent, followed by drying in hot air oven at 40°C. It was coded as SG-*g*-P(NIPAM-*co*-AAM)/Fe_3O_4.

Characterization

The prepared magnetic nanocomposite was characterized by FTIR spectroscopy in wavenumber range of 400-4000 cm^{-1} by using Perkin Elmer Fourier

Transform Infrared Spectrometer. Thermal stability of SG-*g*-P(NIPAM-*co*-AAM) and SG-*g*-P(NIPAM-*co*-AAM)/Fe_3O_4 was compared with sterculia gum using the Perkin Elmer Thermo-gravimetric analyser, TGA 4000. For this the hydrogels were gradually heated under nitrogen atmosphere from ambient temperature upto 700°C at rate of 10 °C/min and loss in weight was recorded. Additionally Differential thermal analysis (DTA) analysis was done under nitrogen atmosphere using DSC 404 F3 (Netzsch) at the scanning speed of 10°C min^{-1} with temperature span of 30°C – 700°C. The magnetic susceptibility of SG-*g*-P(NIPAM-*co*-AAM)/Fe_3O_4 was measured in the range −15,000 to +15,000 Oe using Lake Shore vibrating sample magnetometer (VSM) at room temperature with sensitivity of 10^{-6} emu and 1.5 T magnetic field.

Swelling experiment

In order to evaluate the pH, responsive swelling behaviour of newly fabricated SG-*g*-P(NIPAM-*co*-AAM)/Fe_3O_4, study was done using 50 mg magnetic nanocomposite and buffer solutions (pH 4, 7, 9.2) gravimetrically at 40°C. After definite time period, the magnetic hydrogel samples were taken out and solution cohere to its surface was wiped with tissue paper and then weighed using Shimadzu BL-220H weighing balance. The same course was replicated until a constant weight was attained. All swelling studies were carried out in triplicates. The swelling ratio (SR) of the sample (g/g) was calculated by Eq. (1),

$$SR = \frac{W_t - W_o}{W_o} \quad \ldots(1)$$

Where 'W_0' is the weight of dried and 'W_t' weight of swollen magnetic hydrogel at time't'.

Adsorption experiment

Adsorption capacity of SG-*g*-P(NIPAM-*co*-AAM)/Fe_3O_4 towards dyes MB, MG and CV from their respective aqueous solutions were evaluated as follows. About 20 mg of SG-*g*-P(NIPAM-*co*-AAM)/Fe_3O_4 was added in 20 mL cationic dye solutions (20 mg/L)for 18 h at 35°C. Residual concentration of the cationic dye MG was measured at regular time intervals using Systronics AU-270 UV visible double beam spectrophotometer at corresponding λ_{max} values 617 nm. At equilibrium, the adsorption capacity of magnetic nanocomposite i.e., 'Q_e' (mg/g) was obtained by Eq. (2),

$$\boldsymbol{Q_e = (C_i - C_e) \times \frac{V}{m}} \quad \ldots(2)$$

Here 'C_i' is original and 'C_e' equilibrium concentration of cationic dye solutions (mg/mL), 'm' represents mass of dried adsorbent(g) and 'V' is volume of cationic dye solutions taken (L). The dye adsorption process is illustrated in the Scheme 1. The impact of solution pH on cationic dye adsorption has been measured at pH 4, 7 and 9.2 while that of variation of temperature was evaluated in range of 25- 45°C.

Desorption studies

The reusability of SG-*g*-P(NIPAM-*co*-AAM)/Fe_3O_4 was investigated by carrying out desorption experiment. About 22 mg of dried dye adsorbed magnetic nanocomposite was immersed in 20 mL aqueous solution of pH 1.2 solution for 16 h at 35°C. After due course of time, the supernatant solutions from each slot were pipetted out and absorbance was measured at respective λ_{max} of dye. Amount of dye desorbed in percentage was obtained from Eq. (3) given as below.

$$\text{Desorption \%} = \frac{\text{concentration of dye desorbed (mg/L)}}{\text{concentration of dye adsorbed (mg/L)}} \text{ x } 100 \quad \ldots(3)$$

The reusability studies were repeated for three successive cycles and residual concentration of dye was subsequently determined after each cycle. Statistical analysis of experimental data was performed by Origin (Version 8.0).

Results and Discussion

Synthesis of SG-*g*-P(NIPAM-*co*-AAM)/Fe_3O_4

SG-*cl*-poly(NIPAM-*co*-AAm) was synthesized through free radical graft copolymerization. The

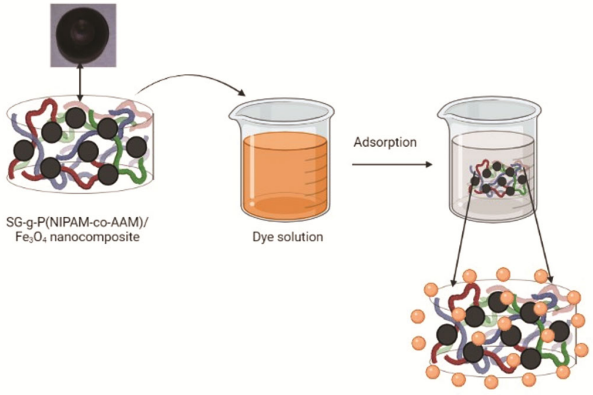

Scheme 1 — Illustration of adsorption of dye using SG-*g*-P(NIPAM-*co*-AAM)/Fe_3O_4.

sulphate anion radicals produced from APS on thermal treatment abstract hydrogen atoms from hydroxyl group of sterculia gum backbone forming macroradicals. This macroradical attacks the monomers AAM and NIPAM forming SG-*g*-P(NIPAM-*co*-AAM). Further crosslinking by MBA among the grafted matrix forms three dimensional crosslinked network. Swelling of dried SG-*g*-P(NIPAM-*co*-AAM) in the solution of $FeCl_2 \cdot 4H_2O$ and $FeCl_3 \cdot 6H_2O$ leads to the diffusion of Fe^{2+} and Fe^{3+} which was visibly monitored by hydrogel colour change from colourless to orange-brown. Further addition of ammonium hydroxide solution resulted in *in situ* formation of Fe_3O_4 nanoparticles in the magnetic hydrogel composite which was indicated by colour change from orange-brown to black. This was designated as SG-g-P(NIPAM-co-AAM)/Fe_3O_4. The various reactions involved in the formation of gel matrix is represented in Scheme 2 and the schematic representation of the procedure of fabrication of SG-*g*-P(NIPAM-*co*-AAM)/Fe_3O_4 is depicted in Scheme 3.

Characterization of SG-*g*-P(NIPAM-*co*-AAM)/Fe_3O_4

FTIR analysis

FTIR analysis was applied to affirm the modification of sterculia gum with monomers AAM and NIPAM and inclusion of Fe_3O_4 nanoparticles. The FTIR spectra of Sterculia gum and functionalised hydrogel is depicted in Fig. 1 (a) and (b), respectively. FTIR of sterculia gum shows peculiar broad band at 3313 cm^{-1} corresponding to hydroxyl groups which is hydrogen bonded. Absorption band observed at 1040 cm^{-1} is because of C–O stretching vibrations in carboxylic acid. In addition, band at 1718 cm^{-1}, 1243 cm^{-1} and 1608 cm^{-1}corresponds to carboxylic acid, acetyl and uronic acid groups present in sterculia gum respectively[25]. In the FTIR spectra of SG-*g*-P(NIPAM-*co*-AAM)/Fe_3O_4 hydrogel, besides other absorption peaks, characteristic band at 3135 cm^{-1} owing to N–H stretching vibrations, 1620 cm^{-1} because of amide C=O stretching vibrations, 1250 cm^{-1} corresponding to C-N stretching have been observed which indicate

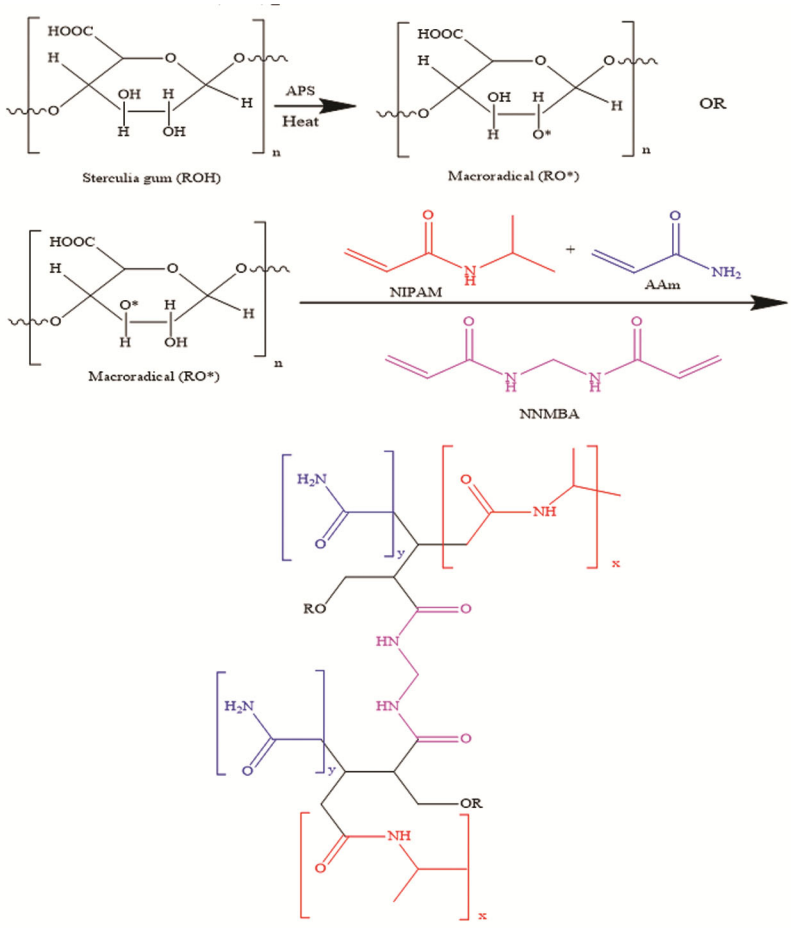

Scheme 2 — Mechanism for the fabrication of SG-g-P(NIPAM-co-AAM)/Fe_3O_4

incorporation of NIPAM and AAM onto the sterculia gum backbone. Apart from this an additional peak at 594 cm^{-1} indicates the presence of Fe_3O_4 within the gel network.

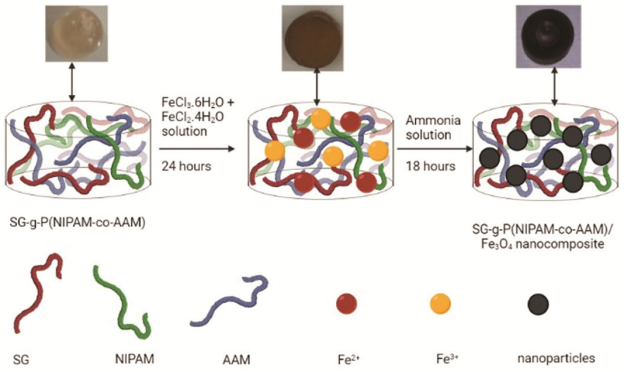

Scheme 3 — Illustration of the fabrication of SG-g-P(NIPAM-co-AAM)/Fe_3O_4

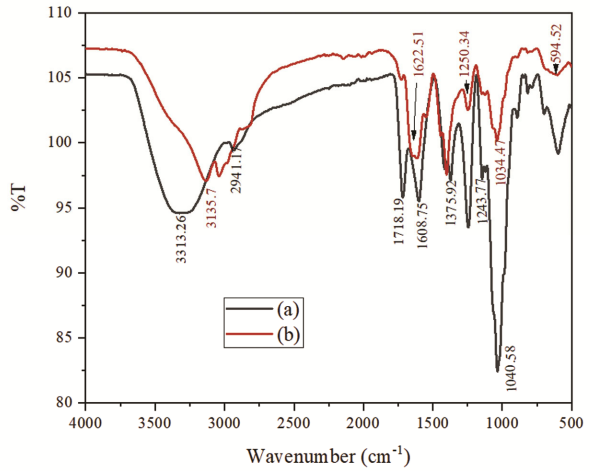

Fig. 1 —FTIR of (a) sterculia gum and (b) SG-*g*-P(NIPAM-*co*-AAM)/Fe_3O_4 gel matrix

Thermogravimetric analysis

Thermogravimetric analysis of sterculia gum and newly fabricated SG-*g*-P(NIPAM-*co*-AAM)/Fe_3O_4 nanocomposite hydrogel was carried out to analyze their thermal stability and the results obtained are depicted in the Fig. 2 (a) and (b), respectively. As evident from Fig. 2a, sterculia gum follows three-step degradation. Initially, 16.59% weight loss occurs due to moisture content in the temperature range of 50-100°C. The gradual degradation of polysaccharide backbone accounts for major weight loss of 48.59% in the temperature range of 250-300°C. The final i.e., third degradation stage led to complete degradation of polysaccharides with weight loss of about 10.02% which begin at approximate 400°C and completes at 650°C. Thermogram of SG-*g*-P(NIPAM-*co*-AAM)/Fe_3O_4 gel matrix represents four stage degradation pattern (Fig. 2b). Functionalized matrix experienced an initial weight loss of 14.88% followed by 21.58% and 20.51% weight loss in second and third stage in the temperature range of 220-330°C and 330-470°C respectively which was due to degradation of crosslinking sites in the gel matrix. Beyond 650°C, an additional weight loss of 6.47% was also reported owing to degradation of grafted side chains. A mass of 36% remains as residue due to the occupancy of magnetite particles which shows that magnetite particles embedded imrpoved the thermal stability of gel matrix.

Differential Thermal Analysis

Differential thermal analysis (DTA) spectra of sterculia gum and SG-*cl*-poly(NIPAM-*co*-AAm)/Fe_3O_4 hydrogel are represented in Fig. 3a and 3b, respectively. As shown in Fig. 3a, an endothermic

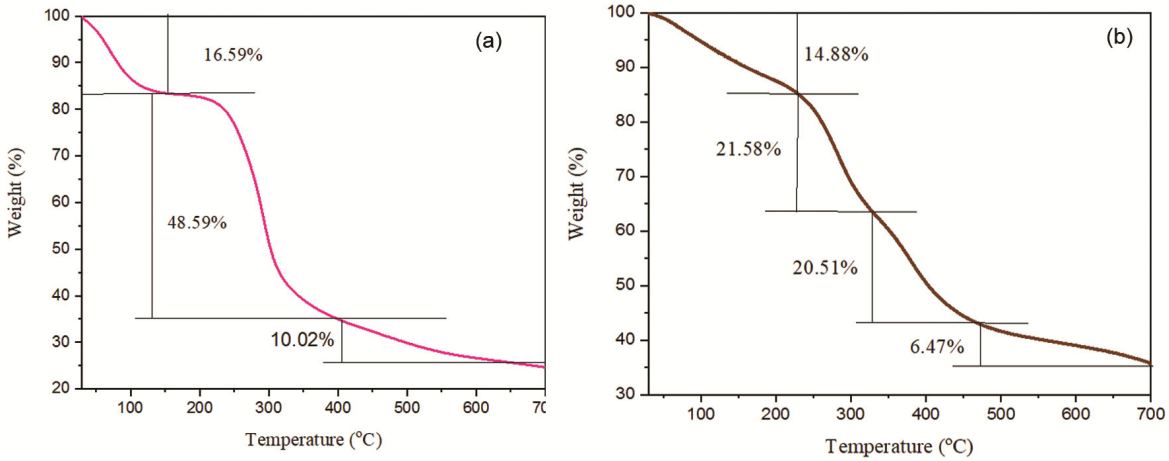

Fig. 2(a) — TGA of sterculia gum

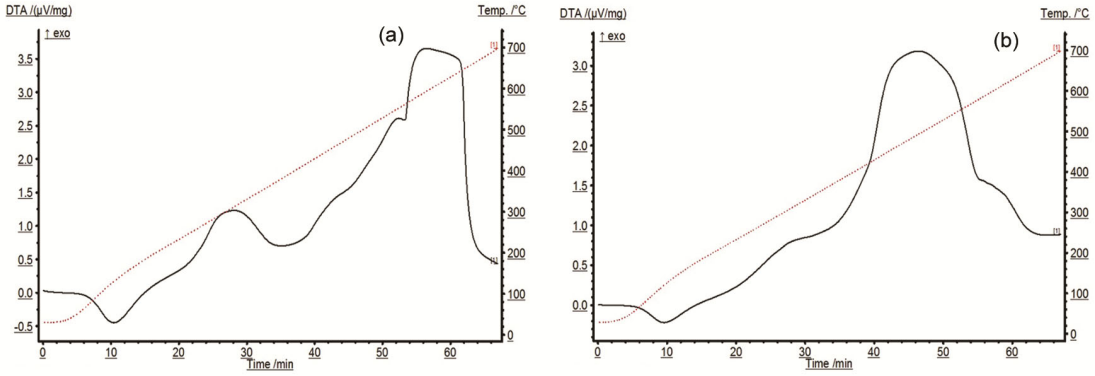

Fig. 3(a) — DTA of sterculia gum

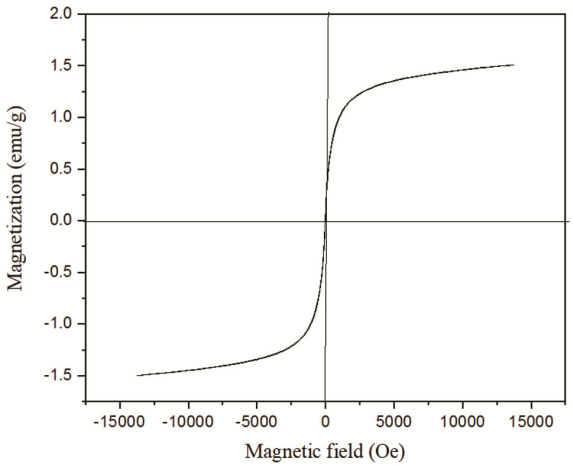

Fig. 4 — Magnetization curve of SG-*g*-P(NIPAM-co-AAM)/Fe_3O_4 gel matrix at room temperature

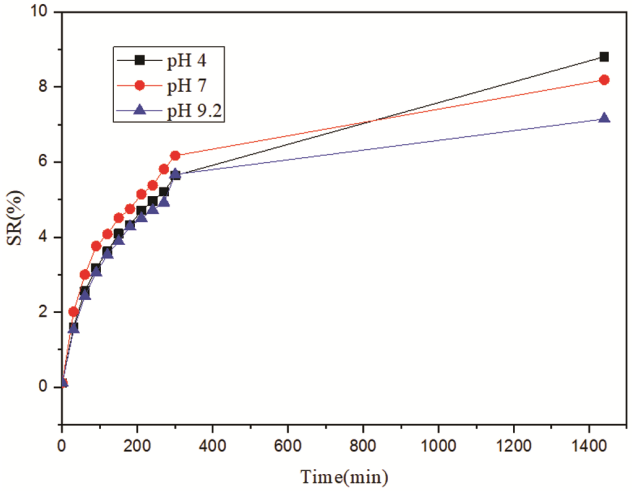

Fig. 5 — Plots of time dependent swelling studies of SG-*g*-P(NIPAM-*co*-AAM)/Fe_3O_4 gel matrix under various pH conditions

peak at 79°C (-0.5 μV) is observed for sterculia gum owing to endothermic discharge of water. Furthermore, appearance of exothermic peaks at 290°C (1.2 μV) and 520°C (2.5 μV) for sterculia gum suggest exothermic degradation of the polysaccharide chain. As evident from Fig. 3b, peak at 79°C (-0.3 μV) owing to endothermic discharge of water from polysaccharides is reported for SG-*cl*-poly(NIPAM-*co*-AAM)/Fe_3O_4. Additionally, presence of exothermic peaks at 280°C (1.1 μV) and 700°C (3.5 μV) suggests exothermic decomposition of the polymer backbone.

Magnetic property measurement

VSM was employed to determine the magnetic characteristics of SG-*g*-poly(NIPAM-*co*-AAM)/Fe_3O_4 hydrogel .The magnetization curve displayed in the Fig. 4 reveals that nanocomposite exhibited superparamagnetic behaviour with zero remanence (residual magnetization) and coercivity (coercive force). The saturation magnetization (Ms) value of 1.5065 emu g^{-1} was observed at ambient temperature which is appreciably smaller as compared literature Ms value for pure Fe_3O_4 particles (66.1 emu g^{-1})[26]. The observed magnetic nature of nanocomposite makes it an attractive material for the elimination of dye as pollutants[27].

Swelling studies SG-*g*-P(NIPAM-*co*-AAM)/Fe_3O_4 hydrogel

The swelling nature of SG-*g*-P(NIPAM-*co*-AAM)/Fe_3O_4 hydrogel was evaluated using buffer of pH 4.0, 7.0 and 9.2.

Swelling of SG-*g*-P(NIPAM-*co*-AAM)/Fe_3O_4 hydrogel in response to time and pH

The swelling ability of newly synthesized SG-*g*-P(NIPAM-*co*-AAM)/Fe_3O_4 hydrogel was studied at pH 4.0, 7.0 and 9.2 for 24 h at 40°C. The results of time dependent swelling studies are shown in Fig. 5. It is observed that the magnetic nanocomposite showed quick uptake of water up to 180 min which

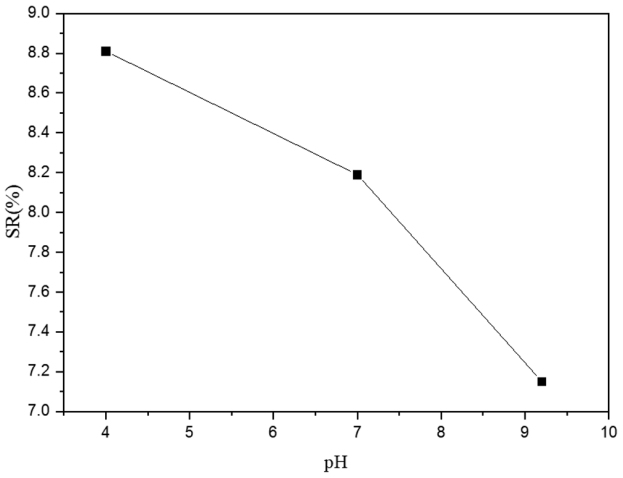

Fig. 6 — Plots of effect of pH for swelling studies of SG-*g*-P(NIPAM-*co*-AAM)/Fe_3O_4 gel matrix under various pH conditions

further continuous gradually and shows maximum swelling ratio of 8.81, 8.19 and 7.15 g/g at pH 4, 7 and 9.2, respectively after 24 h. As observed in the Fig. 6, pH of medium has appreciable impact on the swelling behaviour of the hydrogel. It has maximum swelling ratio at pH 4 corresponding to 8.81 g/g and minimum at pH 9.2 of value 7.15 g/g. The enhanced swelling in acidic medium is due to the existence of Fe_3O_4 nanoparticles in magnetic nanocomposite that reduces possibility of hydrogen bond existence between carboxylic acid of sterculia gum and amide groups of AAM and NIPAM.

Swelling kinetics

Swelling statistics at varied pH solutions were examined by applying first and second order kinetic equations. Swelling as per first order kinetics is expressed in Eq. (4),

$$\frac{dS}{dt} = k_1 (S_{eq} - S) \quad \ldots(4)$$

Where 'S' and 'S_{eq}' are swelling capacities of magnetic nanocomposite at specific time 't' and at equilibrium, respectively, while 'k_1' is the first order rate constant.

Upon integrating Eq. (4) within limits t=0 and S=0,

$$\ln\left(\frac{S_{eq}}{S_{eq} - S}\right) = k_1 t \quad \ldots(5)$$

The second order swelling rate is expressed by Eq. (6),

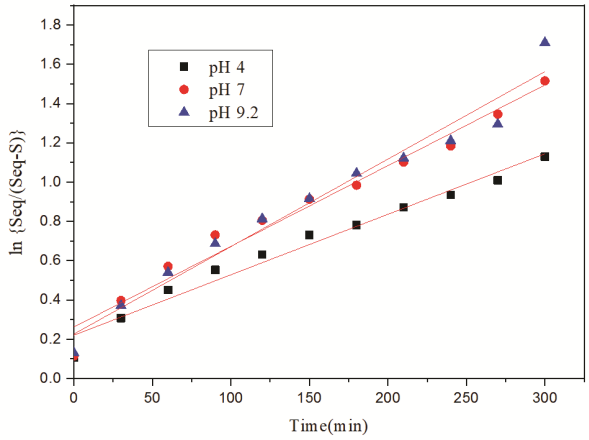

Fig. 7 — Plots of first order kinetic fit for swelling studies of SG-*g*-P(NIPAM-*co*-AAM)/Fe_3O_4 gel matrix under various pH conditions

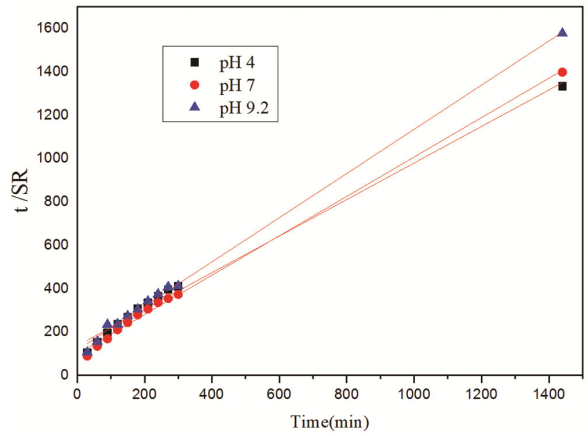

Fig. 8 — Plots of second order kinetic fit for swelling studies of SG-*g*-P(NIPAM-*co*-AAM)/Fe_3O_4 gel matrix under various pH conditions

$$\frac{dS}{dt} = k_2 (S_{eq} - S)^2 \quad \ldots(6)$$

On integrating Eq. (6),

$$\frac{t}{S} = \frac{1}{k_2 Seq^2} + \frac{1}{Seq} t \quad \ldots(7)$$

The graph of $\ln(S_{eq}/(S_{eq}-S))$ against 't' was plotted in accordance with Eq. (5) as shown in Fig. 7 and the results showed poor first order kinetic fit specified by R^2 values of 0.9714, 0.9706 and 0.9635 for solutions of pH 4.0, 7.0 and 9.2, respectively. Consequently, second order kinetics was deployed for analysis of swelling statistics.

The graph of 't/S' versus 't' was plotted in accordance to Eq. (7) as depicted in Fig. 8 and the

Table 1 — Kinetic and diffusion parameter values showing variation of swelling studies of SG-*g*-P(NIPAM-*co*-AAM)/Fe_3O_4 gel matrix at variable pH

	Second order kinetic parameters				Diffusion parameters		
pH	Experimental S_{eq} (g/g)	Calculated S_{eq} (g/g)	K_2 (M^{-1} min^{-1}) 10^{-3}	R^2	k	n	R^2
4.0	1.08	1.18	6.189	0.992	-0.851	0.439	0.957
7.0	1.031	1.1	9.235	0.997	-0.368	0.366	0.928
9.2	0.913	0.981	8.815	0.997	-0.731	0.406	0.901

regression coefficients'S_{eq}'and 'k_2' values are summarized in Table 1 and it is very evident that calculated S_{eq} and experimental values are quite close further affirming that hydrogel swelling obey second order kinetics.

Fickian diffusion model

Nature of diffusion of water into hydrogel was elucidated by Fickian diffusion model which is represented by Eq. (8),

$$f = kt^n \quad \ldots(8)$$

Here, 'f' symbolizes the absorption of water at particular time 't', 'k' as swelling constant varying with structure of hydrogels, while 'n' represents the diffusion exponent. It is documented that for Fickian diffusion, extent of water absorption is directly proportional to square root of time and n=0.5; while in case of non-Fickian diffusion, there is direct relationship between absorption and time with n= 0.5 and 1.0[Ref 28]. 'n' and 'k' values were determined from graph of ln f against ln t (Fig. 9) and values of varied parameters are enlisted in Table 2. It is concluded that as obtained 'n' values are smaller than 0.5 in all cases, process of hydrogel swelling is less Fickian diffusion. This implies that in SG-*g*-P(NIPAM-*co*-AAM)/Fe_3O_4, rate of percolation of water into hydrogel is much lower than amount of relaxation of the polysaccharide chain.

Dye adsorption studies

Dye enrichment studies of SG-*g*-P(NIPAM-*co*-AAM)/Fe_3O_4 shows dependence on feed concentration, adsorbent dose, contact time, pH and temperature. Scheme 4 represents the plausible mechanism of cationic dye adsorption onto surface of SG-*g*-P(NIPAM-*co*-AAM)/Fe_3O_4. Sterculia gum is an anionic hydrocolloid with electrostatic attraction between its carboxylic acid groups and cationic dyes that play pivotal role in the adsorption process. Additionally presence of polar functionalities –OH, -CONH-, -NH_2 on hydrogel results in H-bonding and dipole-dipole interactions with cationic dyes. The three dimensional polymer structure of SG-*g*-P(NIPAM-*co*-AAM) resulting from the van der Walls forces of attraction among non-polar groups restricts the penetration of water molecules in the polymer network. Therefore dye adsorption capacity of SG-*g*-P(NIPAM-*co*-AAM) becomes low. However, incorporation of Fe_3O_4 nanoparticles within parent copolymerized gel increases its surface area thereby increasing the swelling ability and dye adsorption capacity of SG-*g*-P(NIPAM-*co*-AAM)/ Fe_3O_4[29].

Table 2 — Adsorption Kinetic and intraparticle diffusion parameters for adsorption of cationic dye MG on SG-g-P(NIPAM-co-AAM)/Fe_3O_4 gel matrix

Kinetic/isotherm model	Parameters	Value
Pseudo-first order kinetic model	Q_e (calculated) (mg/g)	19.511
	Q_e (experimental)(mg/g)	19.977
	k_1 (10^{-3} min^{-1})	9.673
	R^2	0.994
Pseudo-second order kinetic model	Calculated Qe(mg/g)	25.568
	Experimental Qe (mg/g)	19.977
	K_2 (M^{-1} min^{-1}) 10^{-3}	0.380
	R^2	0.998

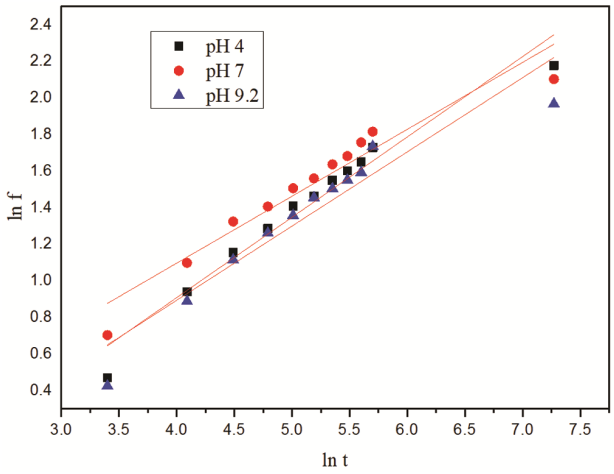

Fig. 9 — Plots of Fickian diffusion model showing variation of swelling studies of SG-*g*-P(NIPAM-*co*-AAM)/Fe_3O_4 gel matrix under various pH conditions

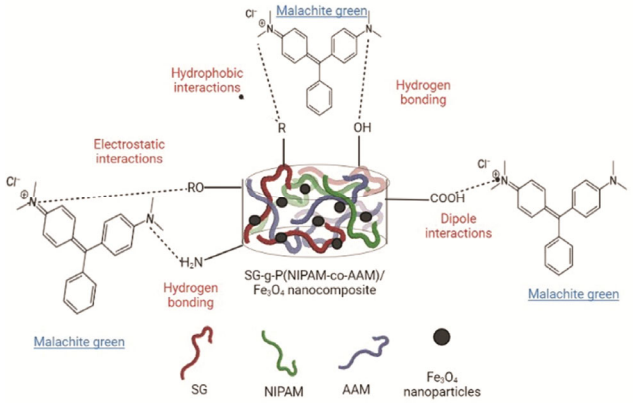

Scheme 4 — Plausible mechanism depicting adsorption of cationic dye MG using SG-g-P(NIPAM-co-AAM)/Fe_3O_4

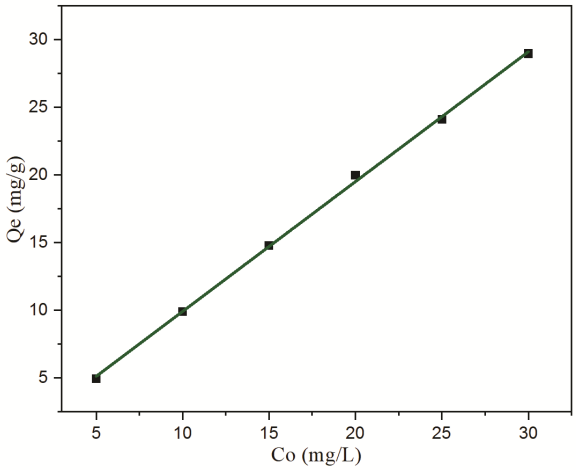

Fig. 10 — Plot of influence of initial cationic dye MG concentration on adsorption on SG-*g*-P(NIPAM-*co*-AAM)/Fe_3O_4 gel matrix

Influence of initial concentration of dye

The influence of initial concentration of dye on adsorption of MG by SG-*g*-P(NIPAM-*co*-AAM)/Fe_3O_4 is displayed in Fig. 10. The experiments were performed with varied concentrations of 5 to 30 mg/L at pH 7.0 and temperature 35°C for 6 h. It was noticed that concentration of the dye adsorbed increases directly with its concentration due to surge in concentration gradient between the dye solution and binding sites of SG-*g*-P(NIPAM-*co*-AAM)/Fe_3O_4.

Influence of adsorbent dose

To judge the impact of adsorbent dose on adsorption capacity of cationic dyes, concentration of SG-*g*-P(NIPAM-*co*-AAM)/Fe_3O_4 was changed in the range of 5-30 mg and immersed in the 20 mL MG dye solution of concentration 20 mg/L at 35°C. The removal efficiency of MG increased when the amount

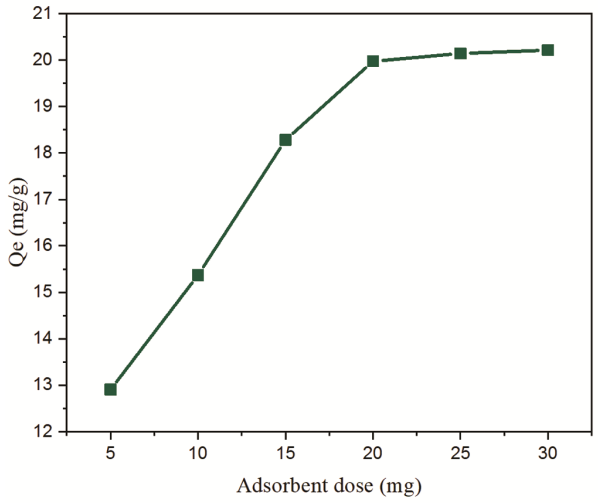

Fig. 11 — Plot of influence of adsorbent dose on MG adsorption on SG-*g*-P(NIPAM-*co*-AAM)/Fe_3O_4 gel matrix

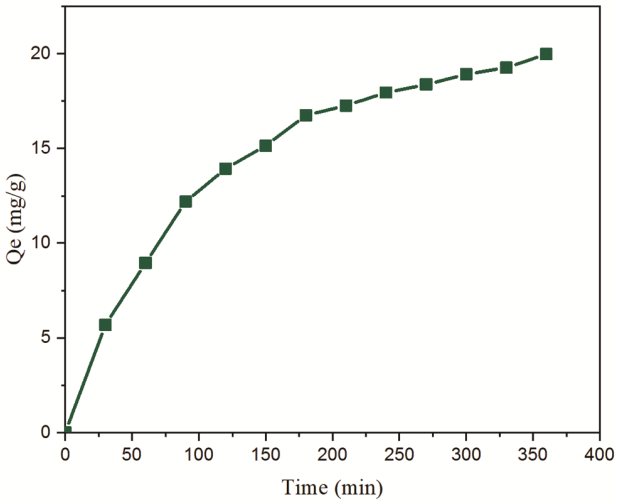

Fig. 12 — Plot of influence of contact time on MG adsorption on SG-*g*-P(NIPAM-*co*-AAM)/Fe_3O_4 gel matrix

of adsorbent increased from 5 mg to 20 mg, as shown in Fig. 11. However, no prominent increase in the adsorption efficiency was noticed with further increase in magnetic nanocomposite concentration. The attainment of equilibrium is attributed to the overloading of adsorption sites to accommodate the increased concentration of cationic dyes in the aqueous solution[30].

Influence of contact time

Fig. 12 depicts influence of contact time on MG adsorption onto the SG-*g*-P(NIPAM-*co*-AAM)/Fe_3O_4 in the range from 0 to 360 min using cationic dye solution of concentration 20 mg/L at 35°C. It was noticed that the dye uptake increases swiftly during

the initial 180 min and then slows gradually over time. About 80% of dye removal was detected during this period. When the equilibrium stage was attained, amount of dye adsorbed Qe was 19.977 (98.78%) for MG suggesting the dye *d*ependent sorption on SG-g-P(NIPAM-*co*-AAM)/ Fe_3O_4.

Kinetics of adsorption

Kinetic models Lagergren pseudo-first-order and Ho pseudo- second order model were employed to scrutinize adsorption mechanism of cationic dye MG onto SG-*g*-P(NIPAM-*co*-AAM)/Fe_3O_4[30,31].

The Lagergren pseudo-first-order model presumes that amount of adsorbate uptake variation is linearly proportional to both differences in saturation concentration as well as quantity of adsorbate uptake with time. The Ho pseudo-second-order kinetics assumes that rate of adsorption is based on the synergy between adsorbent and adsorbate. The integrated forms of Lagergren pseudo-first- order and Ho pseudo-second-order equations are given in Eqs. (9) and (10), respectively.

$$\log (Q_e\text{-}Q_t) = \log Q_e - \frac{k_1 t}{2.303} \qquad (9)$$

$$\frac{t}{Q_t} = \frac{1}{k_2 Qe^2} + \frac{t}{Q_e} \qquad \ldots(10)$$

where Q_e represents dye adsorbed (mg/g) per unit of adsorbent at equilibrium while Q_t at time t(min), respectively, k_1, k_2 indicate rate constants for Lagergren pseudo-first-order (min^{-1}) and Ho for pseudo- second-order adsorption (g mg^{-1} min^{-1}), respectively.

The parameters attained from the linear plots of Eqs (9) and (10) are represented in Table 2, and the linear fitting results obtained from the experimental statistics are depicted, respectively, in Fig. 13 and Fig. 14. The experimental data did not conform to pseudo-first-order kinetic model (Fig. 13), whereas the pseudo-second-order equation showed satisfactory fit to experimental data (Fig. 14) along with good correlation coefficients (R^2, Table 2). These results give inference that adsorption mechanism complies with a pseudo-second-order adsorption model.

Adsorption isotherm model studies

The adsorption isotherms describe the effect of variation of initial concentrations of dye on adsorbent adsorption capacity at equilibrium. To understand plausible interaction among cationic dye and

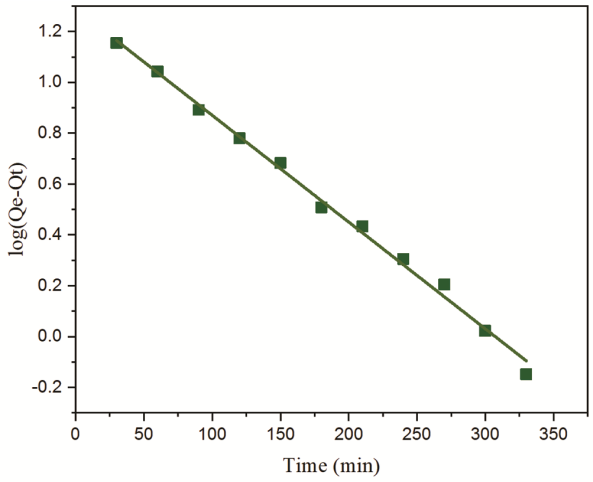

Fig. 13 — Plot of log (Q_e-Q_t) versus time to evaluate pseudo-first order kinetic study for adsorption of MG on SG-*g*-P(NIPAM-*co*-AAM)/Fe_3O_4 gel matrix

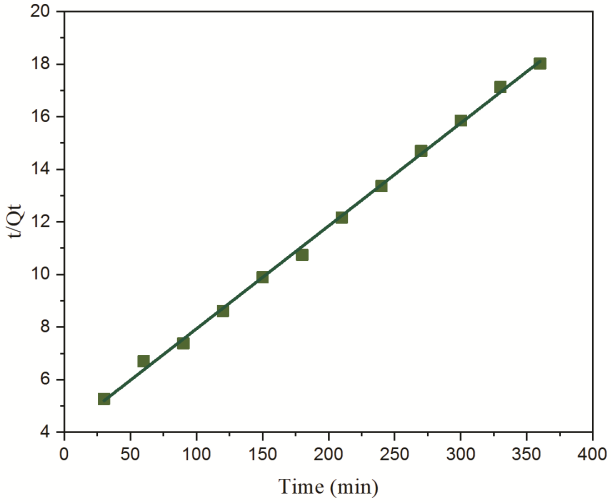

Fig. 14 — Plot of t/Q_t Versus time to evaluate pseudo- second order kinetic study for adsorption of cationic dye MG on SG-*g*-P(NIPAM-*co*-AAM)/Fe_3O_4 gel matrix

magnetic nanocomposite, three adsorption isotherm models, namely Freundlich, Langmuir and Temkin were employed to investigate the statistics for adsorption of the cationic dye on SG-*g*-P(NIPAM-*co*-AAM)/Fe_3O_4.

Freundlich adsorption isotherm is suitable for solutions of low adsorbate concentration and heterogeneous adsorbent surface. It is described by Eq. (12),

$$\log Q_e = \log K_F + 1/n \log C_e \qquad \ldots(12)$$

Here, Q_e is the maximum adsorbate amount adsorbed at equilibrium per unit mass of adsorbent

(mg g^{-1}), C_e represent concentration of adsorbate at equilibrium (mgL^{-1}), K_F indicates adsorption isotherm constant and 'n' is Freundlich coefficient[32]. Freundlich adsorption is favourable only if values of 'n' obtained from intercept of straight line graph of log Q_e against log C_e varies from 1-10.

The Langmuir isotherm implies that surface of adsorbent is homogeneous with definite number of adsorption sites so that a single layer of adsorbate is formed on external area of adsorbent. Langmuir model is given by Eq. (13),

$$\frac{Ce}{Qe} = \frac{1}{Q_m} Ce + \frac{1}{Q_m K_L} \quad \ldots(13)$$

Here, C_e represents concentration of adsorbate at equilibrium (mg L^{-1}), Q_e adsorption capacity of adsorbate at equilibrium (mg g^{-1}), Q_m theoretical saturated adsorption capacity of the monolayer coating (mg g^{-1}) and K_L represents the Langmuir constant. The value of constants Q_m and K_L constants are calculated from slope and intercept of C_e/Q_e versus C_e linear graph. In addition, the utility of an adsorption isotherm is determined from parameter R_L calculated from Eq. (14).

$$R_L = \frac{1}{1+K_L C_o} \quad \ldots(14)$$

where, C_0 represents initial concentration of adsorbent corresponding to the maximal adsorption (mg L^{-1}). If $R_L = 0$, adsorption is irreversible, if $R_L = 1$, linear; if $R_L > 1$, unfavourable; and if $0 < R_L < 1$, favourable. Temkin isotherm model is applied for non uniform surface systems and assumes that heat generated during sorption is dependent on surface area and inversely related to it. Temkin isotherm model is expressed as in Eq. (15),

$$q_e = B \ln A_T + B \ln C_e \quad \ldots(15)$$

where 'B' is Temkin isotherm constant (J $mole^{-1}$) and 'A_T' is constant representing Temkin isotherm equilibrium binding (L g^{-1}).

Fig. 15, 16 and 17 represents Freundlich, Langmuir and Temkin isotherm fit data for the dye enrichment, respectively. The values of different parameters of all three models are enlisted in Table 3. From Table 3, it is evident that R^2 values of Temkin isotherm models is quite higher than Freundlich and Langmuir models for MG. Temkin's results indicate that there may be physical as well as chemical interactions existing between the adsorbent and the adsorbent.

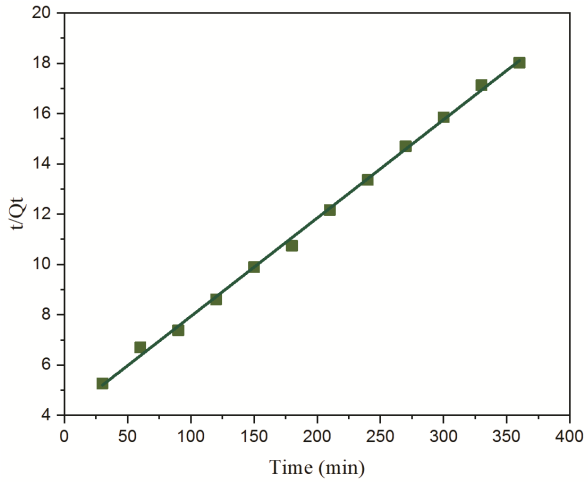

Fig. 15 — Fit of Freundlich model for adsorption of cationic dye MG on SG-*g*-P(NIPAM-*co*-AAM)/Fe_3O_4 gel matrix

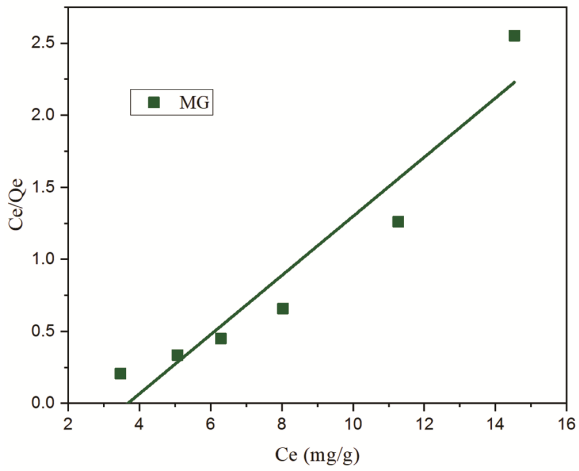

Fig. 16 — Fit of Langmuir model for adsorption of cationic dye MG on SG-*g*-P(NIPAM-*co*-AAM)/Fe_3O_4 gel matrix

Desorption and reusability studies

In order to furnish an efficient, adaptable, and economical system, the crucial parameters are good adsorption efficiency, regeneration and reusability of the used adsorbent. The desorption efficiency and regeneration ability of SG-*g*-P(NIPAM-*co*-AAM)/Fe_3O_4 was performed in aqueous solutions at pH 2 – 11. The maximum desorption was observed at pH 2, while minimum at pH 11. The observation is probably because of existence of H^+ ions in an acidic solution, thereby ensuring ion exchange and facilitating the desorption process. Further SG-*g*-P(NIPAM-*co*-AAM)/Fe_3O_4 was regenerated and adsorption-desorption

Table 3 — Isotherm parameter values for adsorption of MG on SG-*g*-P(NIPAM-*co*-AAM)/Fe_3O_4 gel matrix

Isotherm	Isotherm constant	Value
Freundlich	n	1.384
	K_F (L/g)	47.708
	R^2	0.854
Langmuir	Q_{max} (mg/g)	4.870
	K_L (L/g)	-0.272
	R^2	0.897
Temkin	B	-7.695
	A_T(L/g)	0.0285
	R^2	0.946

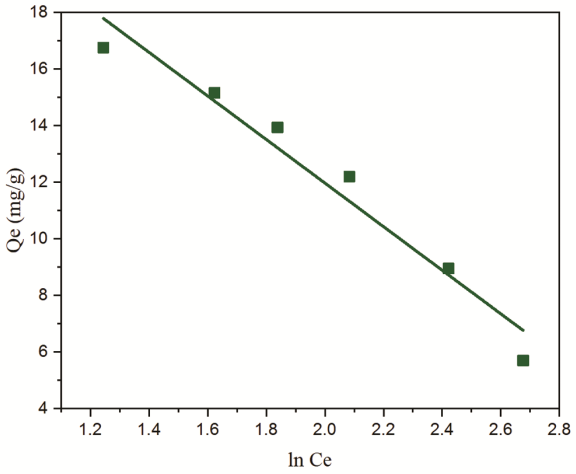

Fig. 17 — Fit of Temkin model for adsorption of cationic dye MG on SG-*g*-P(NIPAM-*co*-AAM)/Fe_3O_4 gel matrix

study for three successive cycles was analyzed as shown in Fig. 18. The desorption was found to be 96.73% for dye MG in the first cycle. It was further ascertained that percentage of dye adsorption reduced slightly for the next two adsorption-desorption cycles owing to utilization of certain sites with cationic functional groups from first desorption cycle. These studies suggest that SG-*g*-P(NIPAM-*co*-AAM)/Fe_3O_4 is an effective adsorbent for speedy separation of cationic dyes from the aqueous solution.

Conclusion

In the present study, a novel magnetic nanocomposite adsorbent SG-*g*-P(NIPAM-*co*-AAM)/Fe_3O_4 has been synthesized by graft copolymerization and by in situ integration of nanomagnetite components. The FTIR, TG-DTA, as well as VSM studies confirm the presence of magnetite nanoparticles inside gel matrix. The synthesized nanocomposite displayed ferromagnetic tendency along with saturation magnetization of 1.5065 emu g^{-1}. The MG dye uptake using the synthesized nanocomposite was determined under

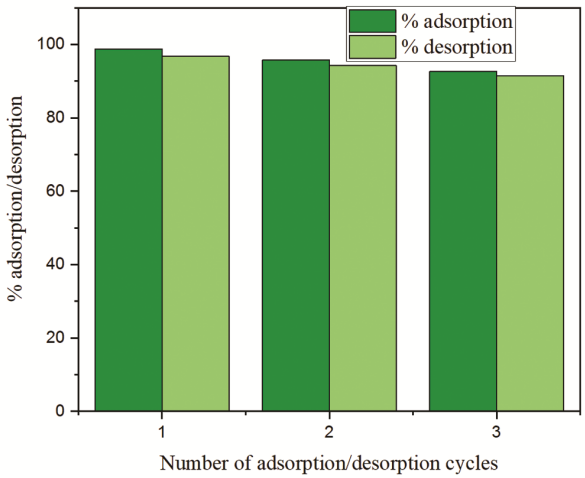

Fig. 18 — Three consecutive cycles of adsorption/desorption ofcationic dye MG on SG-*g*-P(NIPAM-*co*-AAM)/Fe_3O_4 gel matrix

diverse conditions and isotherm as well as kinetic parameters were demonstrated. The adsorption of dyes on SG-*g*-P(NIPAM-*co*-AAM)/Fe_3O_4 followed Temkin isotherm model and well-illustrated by pseudo second order kinetic model. The regeneration ability of adsorbents and excellent recovery have shown its optimistic application for water restoration.

Acknowledgement

The authors are grateful to the Department of Physical Sciences, Sant Baba Bhag Singh University, and Department of Chemistry, Kanya Maha Vidyalaya, (Jalandhar) for the laboratory facilities and S. N. Bose National Centre for Basic Sciences, Kolkata and Lovely Professional University, Phagwara for the technical support.

References

1 Kumari K & Abraham T E, *Bio resource Technol*, 98 (2007) 1704.
2 Bagheri N, Lakouraj M M, Hasantabar V & Mohseni M, *J Hazard Mater*, 403 (2021) 123631.
3 Rosa J M, Garcia V S G, Boiani N F, Melo C G, Pereira M C C & Borrely S I, *J Environ Chem Eng*, 7 (2019) 102973.
4 Saruchi & Kumar V, *Arab J Chem*, 12 (2019) 316.
5 Srivastava S, Sinha R & Roy D, *Aquat Toxicol*, 66 (2004) 319.
6 Fernandes C, Lalitha V S & Rao V K, *J Carcinog*, 12 (1991) 839.
7 Rao K V K, *Toxicol Lett*, 81 (1995) 107.
8 Sun S, Zhu L, Liu X, Wu L, Dai K, Liu C, Shen C, Guo X, Zheng G & Guo Z, *ACS Sustain Chem Eng*, 6 (2018) 9866.
9 Hao O J, Kim H & Chiang P C, *Crit Rev Environ Sci Technol*, 30 (2000) 449.
10 Mittal H, Maity A & Ray S S, *Int J Biol Macromol*, 79 (2015) 8.

11 Mittal A, Ahmad R & Hasan I, *Desalin Water Treat*, 57 (2016) 15133.
12 Fan L, Luo C, Sun M, Li X, Lu F & Qiu H, *Bioresource Technol*, 114 (2012) 703.
13 Chang Y C & Chen D H, *J Colloid Interface Sci*, 283 (2005) 446.
14 Zhou Y T, Nie H L, Branford-White C, He Z Y & Zhu L M, *J Colloid Interface Sci*, 330 (2009) 29.
15 Gong J L, Wang B, Zeng G M, Yang C P, Niu C G, Niu Q Y, Zhou W J & Liang Y, *J Hazard Mater*, 164 (2009) 1517.
16 Xu Y Y, Zhou M, Geng H J, Hao J J, Ou Q Q, Qi S D, Chen H L & Chen X G, *Appl Surf Sci*, 258 (2012) 3897.
17 Xu J, Zhang F, Sun J, Sheng J, Wang F & Sun M, *Molecules*, 19 (2014) 21506.
18 Lin D D, *RSC Adv*, 9 (2019) 3625.
19 Mittal H, Parashar V, Mishra S B, Mishra A K & Elsevier B V, *Chem Eng J*, 255 (2014) 471.
20 Hasan I, Bhatia D, Walia S & Singh P, *Groundw Sustain Dev*, 11 (2020) 100378.
21 Hosseinzadeh H & Ramin S, *Int J Biol Macromol*, 106 (2018) 101.
22 Li K, Yan J, Zhou Y, Li B & Li X, *J Mol Liq*, 335 (2021) 116291.
23 Anderson D M W, Mcnab C N B, Anderson C G, Brown P M & Pringuer M A, *Int Tree Crops J*, 2 (1982) 147.
24 Reddy N N, Mohan Y M, Varaprasad K, Ravindra S, Joy P A & Raju K M, *J Appl Polym Sci*, 122 (2011) 1364.
25 Singh R, Pal D, Mathur A, Singh A, Krishnan M A & Chattopadhyay S, *React Funct Polym*, 144 (2019) 104346.
26 Reddy N N, Mohan Y M, Varaprasad K, Ravindra S, Joy P A & Raju K M, *J Appl Polym Sci*, 122 (2011) 1364.
27 Prajwal K & Vishalakshi B, *Int J Biol Macromol*, 156 (2020) 1408.
28 Jana S, Pradhan S S & Tripathy T, *J Polym Environ*, 2 (2017) 1.
29 Zeng Q , Qi X, Zang M, Tong X, Jiang N, Pan W, Xiong W, Li Y, Xu J, Shen J & Xu L, *Int J Biol Macromol*, 145 (2020) 1049.
30 Arous N A & Djadoun S, *Macromol Symp*, 303 (2011) 123.
31 Cert D L, Irinei F & Muller G, *Carbohydr Polym*, 13 (1990) 375.
32 Mittal H, Maity A & Ray S S, *J Phys Chem B*, 119 (2015) 2026.